IEEE Access
Multidisciplinary | Rapid Review | Open Access Journal

Received April 26, 2017, accepted May 8, 2017, date of publication May 16, 2017, date of current version June 28, 2017.

Digital Object Identifier 10.1109/ACCESS.2017.2704523

A Novel Low-Loss Millimeter-Wave 3-dB 90° Ridge-Gap Coupler Using Large Aperture Progressive Phase Compensation

MOHAMMADMAHDI FARAHANI[1], (Student Member, IEEE), MOHAMMAD AKBARI[2], (Student Member, IEEE), MOURAD NEDIL[3], (Senior Member, IEEE), TAYEB A. DENIDNI[1], (Senior Member, IEEE), AND ABDEL R. SEBAK[2], (Fellow, IEEE)

[1]Institut National de la Recherche Scientifique, Université du Québec, Montreal, QC H5A 1K6, Canada
[2]Electrical and Computer Engineering Department, Concordia University, Montreal, QC H4B 1R6, Canada
[3] Université du Québec en Abitibi-Témiscamingue, Rouyn-Noranda, QC J9P 1Y3, Canada

Corresponding author: Mohammadmahdi Farahani (mohammadmahdi.farahani@emt.inrs.ca)

ABSTRACT A novel millimeter-wave (mm-wave) 90° phase-compensated hybrid coupler using the ridge-gap waveguide (RGW) technology is studied and developed. The coupler is low-loss at mm-wave frequency bands, whereas using conventional transmission lines, such as microstrip or substrate integrated waveguides, yields relatively a high amount of insertion loss. The proposed coupler is designed using large coupling apertures, which with their phase variation over the apertures can compensate for the progressive phase of the coupler and achieve a low output-phase error. The ridge-gap 3-db 90° hybrid coupler is suitable for designing mm-wave beamforming networks, such as the Butler matrix beamformer, where the cross-over transmission lines present a difficulty in designing such networks. In this paper, the dispersion diagram of the RGW is extracted, and a multicoupling aperture technique is formulated for designing the coupler. The coupler is fabricated and measured. The simulated and measured results show a good agreement.

INDEX TERMS mm-wave, phase compensation, dispersion diagram, coupler.

I. INTRODUCTION

Due to a small dimension and high amount of propagation loss at mm-wave frequencies, designing beamforming networks at mm-wave frequency range has been a challenging task for designers. In the past decade, there were several efforts to invent a new low-loss high-efficiency transmission line for high frequency microwave and mm-wave frequency ranges. For instance, the substrate integrated waveguide (SIW) technology was developed in the past decade as a low-loss transmission line [1]–[3]. However, designing the microwave components, such as couplers with SIW technology, deteriorates the low-loss performance of the SIW transmission line, because of disturbing the host SIW transmission line characteristic [4]–[6].

To overcome these problems another alternative approach called ridge-gap waveguide technology has been proposed [7]. Ridge-gag waveguide is an extremely low-loss transmission line at mm-wave frequencies [7]–[9]. In this technology, the electric and magnetic fields are captured between two metal surfaces and two open side walls. By embedding some structure like a bed of nails along the two open sides, a band-gap is obtained in x and y-directions, as illustrated in Fig. 1. Therefore the electric and magnetic fields are travelling in the air gap (Fig. 1(b)). In the ridge-gap transmission line, losses are smaller than SIW transmission line due to that the electric and magnetic waves are travelling in the air and host dielectric in the ridge-gap and SIW transmission lines, respectively. Moreover, implementing bend, slot or any disturbance in SIW transmission line deteriorates the low-loss characteristic nature of it, because of disturbing the host SIW transmission line characteristic. However, the ridge-gap transmission line is less sensitive to disturbance such as bend or slot. For instance, in both SIW and ridge-gap, the loading effect of a bend in the transmission line will be compensated, but the difference comes from the fact that SIW is filled with dielectric, which has electric

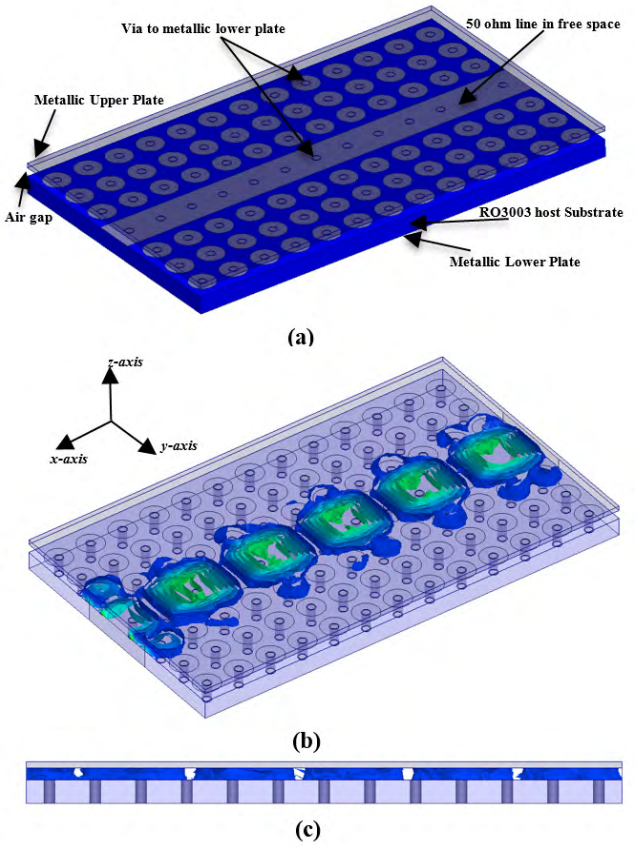

FIGURE 1. (a) Proposed ridge-gap waveguide. (b) Travelling electric fields in the air gap. (c) Side view of travelling electric fields in the air gap.

and magnetic losses. In both SIW and ridge-gap, the loading effect of the bend is compensated by truncating the corner, but the wave will reflect several times at the corner. These reflected waves in SIW and ridge-gap are travelling in air and host dielectric, respectively, which make the SIW more lossy to the disturbance in the transmission line.

Several techniques have been introduced in the literature to design a low-loss 3dB 90° hybrid coupler, such as SIW branch line couplers [5] and [10], and a two-layer SIW coupler [11]. These techniques are high-loss at mm-wave frequency range. Another problem with these techniques is a high amount of output phase error which comes from the progressive phase nature of them.

In this paper, a low-loss multi-aperture 3dB 90° hybrid coupler with ridge-gap technology is designed and fabricated. The coupler has a very low amount of output-phase error. This is achieved by considering the fact that Bethe's small coupling aperture theory [12], cannot show an exact expression for large square aperture in a multi-aperture coupler. In the case of large square aperture, the coupling and isolation coefficients are frequency dependent and the phase varies over the large coupling aperture, which can be used to compensate for the progressive phase nature of the coupler. In Section II, the host RGW transmission line and the transition method to microstrip are explained. In Section III, the theory of the proposed phase compensated six-stage hybrid coupler is

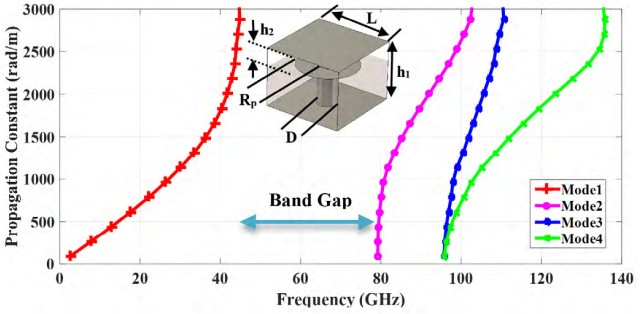

FIGURE 2. Dispersion diagram of the periodic unit cell of mushroom-like ridge. The unit cell dimensions are $D = 0.25mm$, $R_p = 0.38mm$, $L = 1mm$, $h_1 = 0.5mm$, $h_2 = 0.25mm$.

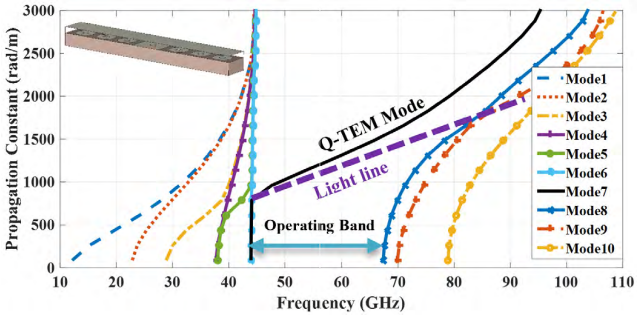

FIGURE 3. Dispersion diagram of the proposed ridge-gap waveguide in Fig.1.

studied and developed. The proposed coupler is designed and discussed in Section IV. In section V, experimental results are measured and compared to the simulated ones.

II. RIDGE-GAP WAVEGUIDE AND TRANSITION TO MICROSTRIP

The proposed ridge-gap waveguide is shown in Fig. 1. The electric and magnetic fields are captured between two metal surfaces and two open side walls. By embedding some structure like a bed of nails along the two open sides, a band-gap is obtained in x and y-directions. The dispersion diagram of the ridge-gap unit cell, and the dispersion diagram of the ridge-gap transmission line of Fig. 1 are carried out with CST, and are shown in Fig. 2 and Fig. 3, respectively. As it can be seen from Fig. 3, there is a band-gap between 45GHz to 68GHz. Only the Q-TEM mode can propagate at this band-gap. The ridge-gap waveguide operates based on the concept of PEC-over-PMC plates to kill global TEM modes in a parallel-plate waveguide (PEC-over-PEC), and has the unique property of simultaneous propagation of several independent degenerate local quasi-TEM (Q-TEM) waves. In the longitudinal direction, it works as a PMC plate in the direction transverse to the strips. Thereby, PEC-over-hard surface plates can be seen as PEC-over-PMC plates in the transverse direction and as PEC-over-PEC plates in the longitudinal direction. As a result, any kind of propagation is suppressed except for the TEM-like propagation along the strips, i.e., there will only exist quasi-TEM waves propagating along the strips. Therefore, the electric and magnetic fields can travel in the air gap as illustrated in Fig. 1(b).

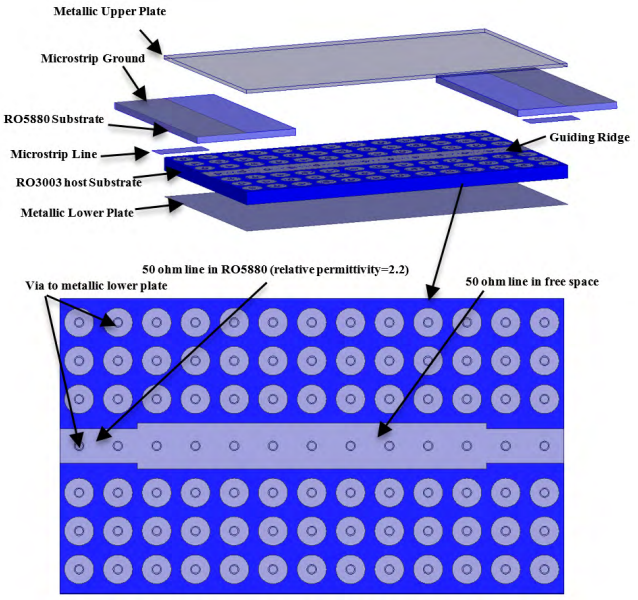

FIGURE 4. Ridge-gap waveguide transition to microstrip waveguide.

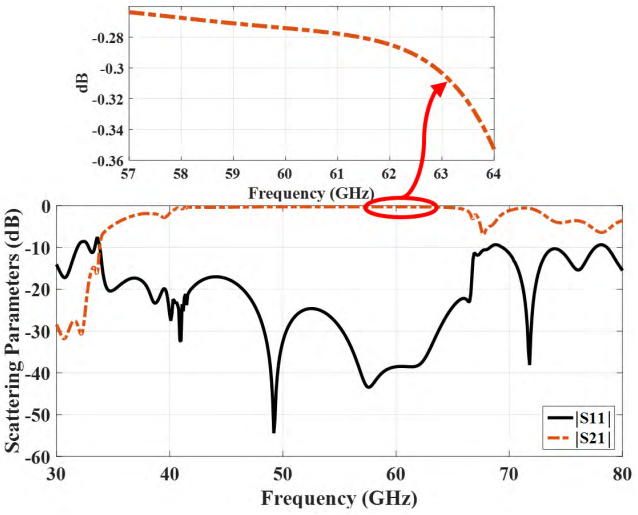

FIGURE 5. Simulated scattering parameters of the proposed transition from microstrip to ridge-gap waveguide in Fig. 4.

The presented technique in [9], is used for the transition from the microstrip line to ridge-gap waveguide. The transition is shown in Fig. 4. The characteristic impedance of the designed ridge-gap waveguide in Fig. 4 is 50 ohm. The scattering parameters of the transition in Fig. 4 are carried out with HFSS, and are shown in Fig. 5.

III. THEORY OF PHASE COMPENSATED SIX STAGE 90° HYBRID COUPLER

The series coupling slot technique is used for designing a 3dB coupler, as shown in Fig. 6. There are several techniques to increase the operating bandwidth of couplers, such as using multiple series coupling slots [13]. The conventional theory in the literature for designing multi-hole directional

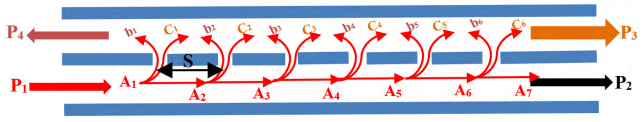

FIGURE 6. Geometry of the proposed six stage coupler.

couplers [13] assumes that the input power of feeding waveguide is constant over all of holes because of its small amount of coupling at the holes. However, this is not correct in the case of very tight coupling above −10dB, since most of the input power leaking to the coupled waveguide due to the large amount of coupling at the holes. By considering the six-slot coupling aperture structure in Fig. 6, we can define the forward and backward coupled power components in the upper waveguide, as shown in Fig. 6. The forward and backward coupled power can be calculated as

$$P_2 = A_7 \tag{1}$$

$$P_3 = \sum_{n=1}^{n=6} A_n C_n e^{-j\beta(6-n)S} \tag{2}$$

$$P_4 = \sum_{n=1}^{n=6} A_n b_n e^{-j\beta(n-1)S} \tag{3}$$

where A_n is defined as

$$A_n = \begin{cases} P_1, & n = 1 \\ P_1 e^{-j(n-1)\beta S} \times \prod_{i=1}^{n-1} (1 - b_i - C_i), & n = 2, 3, 4, 5, 6, 7 \end{cases} \tag{4}$$

For small apertures, the coupling and isolation coefficients (C_n and b_n) are frequency-independent quantities [12]. Square apertures are narrowband and high coupling structures compered to small apertures. But Bethe's small coupling aperture theory [12] cannot show an exact expression for large square aperture in a multi-aperture coupler. In the case of large square aperture, the coupling and isolation coefficients (C_n and b_n) are defined by [12]:

$$C_n = b_n = 0.508 \times W_s^3 \times \frac{\tan\left(\frac{\pi f}{2f_{co}}\right)}{\frac{\pi f}{2f_{co}}} e^{\left(-\frac{2\pi h_m f_{co} Q}{C_0}\sqrt{1-\left(\frac{f}{f_{co}}\right)^2}\right)} \tag{5}$$

The first term is given by Cohn [14], which takes into account the effect of aperture resonant frequency (f_{co}). The exponential term is the correction factor for thickness of the coupling wall (h_m), and Q is an empirical parameter that models the apparent extra electrical thickness of the coupling wall. For circular apertures, Q is given by [14] as

$$Q = \frac{\alpha D}{h_m} + 1 \tag{6}$$

where D is the hole diameter, and α is a constant value (0.065). This expression is not accurate for a large square aperture. To correct Q, the different aperture widths are simulated with HFSS and the bellow equation for Q is fitted to

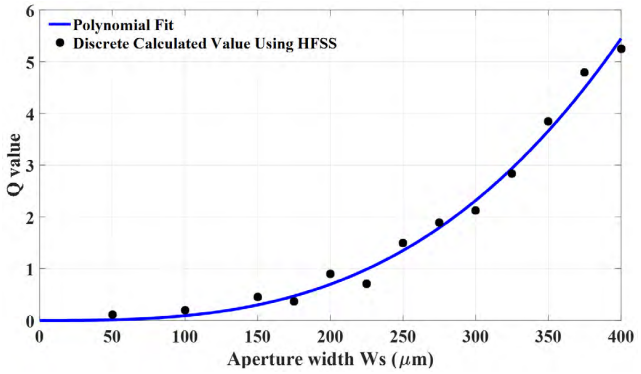

FIGURE 7. Calculated discrete corrected *Q* factor and polynomial fit.

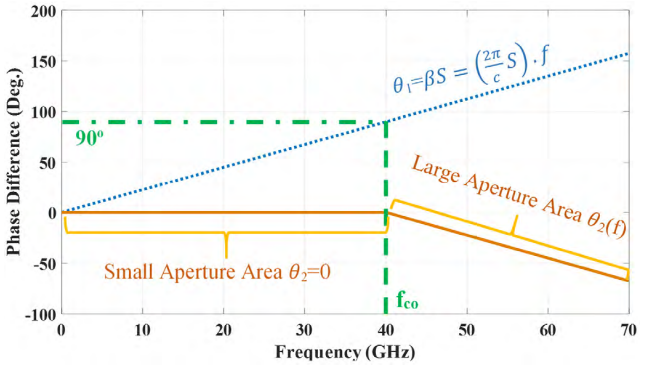

FIGURE 8. Large coupling aperture output phase difference. It is divided into two terms, the linear output phase difference (θ_1) and the large coupling aperture output phase error (θ_2). θ_2 in (12) is not straight line like the ideal θ_2 which is plotted in this figure.

a polynomial functional form depending on the aperture size as

$$Q = 0.02768W_s^3 - 0.27583W_s^2 + 0.85232W_s + 0.97261 \tag{7}$$

where W_s is the aperture width in μm, and the coupling wall thickness (h_m) is considered 0.127mm. The calculated discrete corrected Q factor and polynomial fit are shown in Fig. 7. The coupling of the structure is calculated in Appendix-A and can be defined as (8), shown at the bottom of this page.

The phase difference between the two output ports (θ) is

$$\theta = \angle\,(P_3/P_2) \tag{9}$$

The output phase difference can be simplified as

$$\theta = \theta_1 + \theta_2 \tag{10}$$

which can be divided into two terms, the linear output phase difference (θ_1) and the large coupling aperture output phase error (θ_2). These two are calculated in Appendix-B and are given in (11) and (12), as shown at the bottom of this page.

The calculated θ_1 and θ_2 using (11) and (12) are plotted using Matlab, and are shown in Fig. 8 versus frequency. The large coupling aperture output-phase error (θ_2) is zero for the frequency lower than f_{co}. For the frequency higher than f_{co}, it has a negative slope which can compensate for the positive slope of θ_1. As a result, a very flat output phase difference can be achieved for frequencies higher than f_{co} if θ_1 and θ_2 have the same slope magnitude with different sign like the ideal scenario showed in Fig. 8. However, θ_2 in (12) is not straight line like the ideal θ_2, which is plotted in Fig. 8 for frequencies higher than f_{co}. The real θ_2 is plotted using HFSS for a typical aperture to show the real behavior of θ_2 (Fig. 9). f_{co} defines the border between a small aperture area and a large aperture area. In a small aperture area, there is not any phase variation over the aperture. In other words, in small apertures, the coupling and isolation coefficients (C_n and b_n) are frequency-independent quantities [12]. f_{co} is affected by the aperture length (L_s) and aperture width (W_s). However, by considering that the aperture length (L_s) is five times bigger than the aperture width (W_s), f_{co} is mostly affected by the aperture length (L_s). The design procedure for the coupler

$$Coupling = 10\log\left|\frac{1-\left(1-1.016\times W_s^3\times\frac{\tan\left(\frac{\pi f}{2f_{co}}\right)}{\frac{\pi f}{2f_{co}}}e^{\left(-\frac{2\pi h_m f_{co} Q}{C_0}\sqrt{1-\left(\frac{f}{f_{co}}\right)^2}\right)}\right)^6}{2}\right| \tag{8}$$

$$\theta_1 = \beta S \tag{11}$$

$$\theta_2 = \angle\left(\frac{1-\left(1-2\times0.508\times W_s^3\times\frac{\tan\left(\frac{\pi f}{2f_{co}}\right)}{\frac{\pi f}{2f_{co}}}e^{\left(-\frac{2\pi h_m f_{co} Q}{C_0}\sqrt{1-\left(\frac{f}{f_{co}}\right)^2}\right)}\right)^6}{2\left(1-2\times0.508\times W_s^3\times\frac{\tan\left(\frac{\pi f}{2f_{co}}\right)}{\frac{\pi f}{2f_{co}}}e^{\left(-\frac{2\pi h_m f_{co} Q}{C_0}\sqrt{1-\left(\frac{f}{f_{co}}\right)^2}\right)}\right)^6}\right) \tag{12}$$

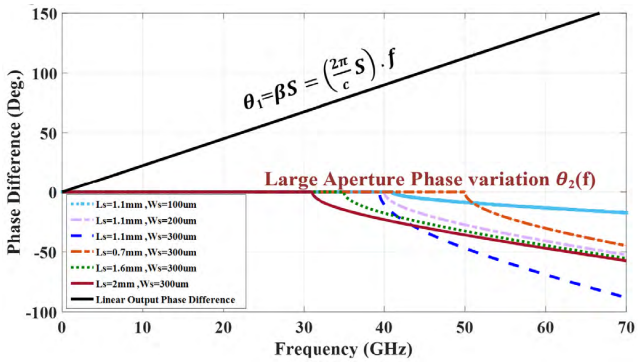

FIGURE 9. Simulated phase difference using HFSS for different values of W_s and L_s. We considered that the distance between apertures (S) is 1.875mm, and the coupling wall thickness (h_m) is 0.127mm.

is explained in next section. The coupler, which is defined in the next section, is simulated using HFSS. Fig. 9 shows the simulated phase difference for different values of W_s, L_s, θ_1 and θ_2. We considered that the distance between apertures (S) is 1.875mm and the coupling wall thickness (h_m) is 0.127mm. As it can be seen from Fig. 9, the aperture resonant frequency (f_{co}) is mostly affected by the aperture length (L_s). Changing the aperture length (L_s) will also affect the slope of the θ_2. It is also can be seen that the slope of θ_2 is proportional to the aperture width (W_s), but it does not have a significant impact on the aperture resonant frequency (f_{co}). The slope of θ_2 increases by increasing W_s. We expected this behavior because of the fact that by reducing W_s, the coupling strength of the aperture will be reduced and it will act like a small coupling aperture with frequency independence.

IV. DESIGN OF THE PROPOSED COUPLER

The above mentioned theory is used to calculate the initial value for the coupling aperture size of the proposed six stage coupler. The final schematic of the coupler based on the ridge-gap technology is shown in Fig. 10. The coupling aperture dimensions are indicated in Fig. 10. The thickness of the coupling aperture wall is considered 0.127mm, and then Q factor is estimated by (7). In the previous section, it is shown that in large coupling apertures at the frequencies higher than f_{co}, θ_2 has a negative slope, which can compensate for the positive slope of θ_1. As it is shown in the previous section, the aperture resonant frequency (f_{co}) is mostly affected by the aperture length (L_s), and it is also shown that the slope of θ_2 is proportional to the aperture width (W_s), but it does not have a significant impact on the aperture resonant frequency (f_{co}) (Fig. 9). Moreover, the total coupling can be calculated by (8), which is a function of the aperture width (W_s) and the aperture resonant frequency (f_{co}) directly, and it is absolutely a function of the coupling wall thickness (h_m), which is considered to be 0.127mm. The coupling is not directly a function of the aperture length (L_s); however, the aperture resonant frequency (f_{co}) is effectively affected by the aperture length (L_s). Moreover, the coupling is a function of Q factor, and the Q factor is a function of the coupling wall thickness (h_m) and the aperture width (W_s). However, in this work, the Q factor is estimated for a fixed value of h_m that is equal to 0.127mm.

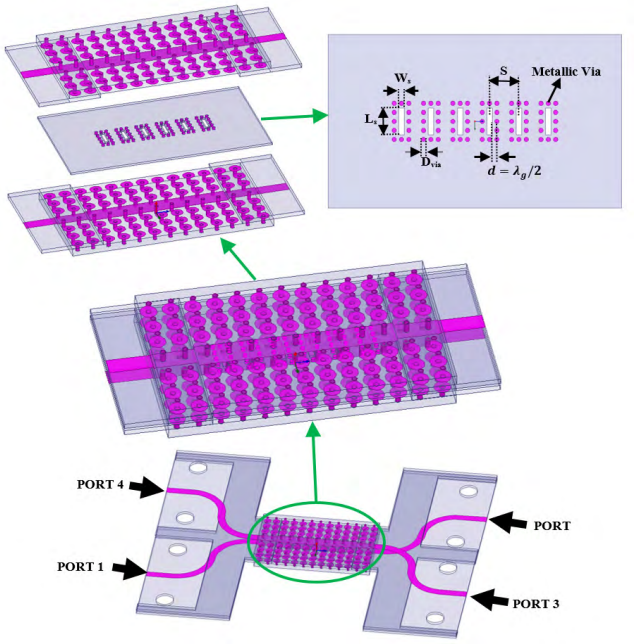

FIGURE 10. Geometry of the proposed two layer 3dB 90° hybrid coupler. ($W_s = 0.35mm$, $L_s = 1.2mm$, $D_{via} = 0.3mm$, $D = 0.52mm$).

The first step for designing the proposed coupler is selecting the proper values for the aperture width (W_s) and the aperture length (L_s) in a way which θ_2 has the same slope magnitude like as θ_1 with different signs, to compensate for the progressive phase of θ_1 and to obtain a very flat phase response. On the other hand, W_s and L_s will affect the amount of the coupling. However, the effect of L_s on the coupling is through the aperture resonant frequency (f_{co}) that is much less compared to the aperture width (W_s). Thus, at first the proper value is selected for W_s to give us the 3dB coupling. After that, by optimizing L_s and S (aperture spacing), the proper values for L_s and S can be chosen to compensate for the progressive phase of θ_1 by θ_2 and satisfied the condition of $\theta_1\,(f_{co}) = 90°$. Applying this procedure, the aperture dimensions are founded as $W_s = 0.35mm$, $L_s = 1.2mm$ and $S = 1.875mm$.

In (5), the coupling and isolation coefficients (C_n and b_n) are given for a completely PEC coupling wall [12], but in our design, Rogers RO3003 is used as a coupling wall. The upper and lower sides of the coupling wall are PEC, but four sides on the aperture, between the upper and lower sides are not PEC (Fig. 11(a)). If we consider the coupling wall as a parallel PEC waveguide, filled by RO3003 substrate, the following equation can be written for a shorted waveguide (Fig. 11(b))

$$Z_z = \frac{E_z}{H_Y} = j\left(\frac{W}{P}\right)\eta \tan k_g d \tag{13}$$

The surface impedance on the edge is zero when $d = \lambda_g/2$, which corresponds to a PEC wall as indicated in Fig. 11(c). λ_g is the wavelength in the parallel plate waveguide filled with RO3003 substrate.

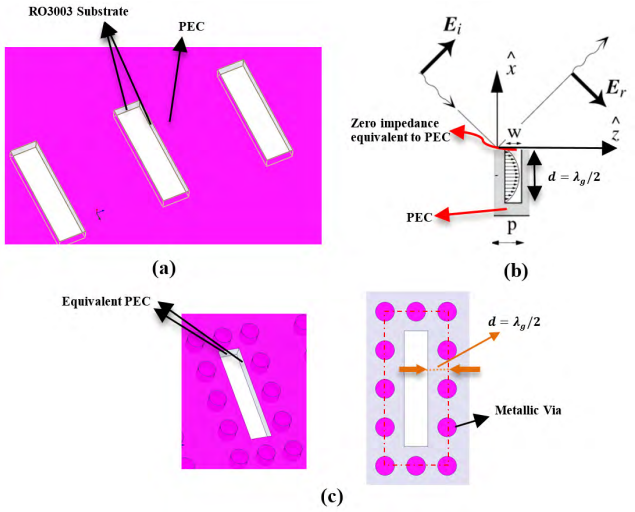

FIGURE 11. PEC coupling aperture composes of $\lambda_g/2$ shorted parallel plate waveguide filled with RO3003 substrate.

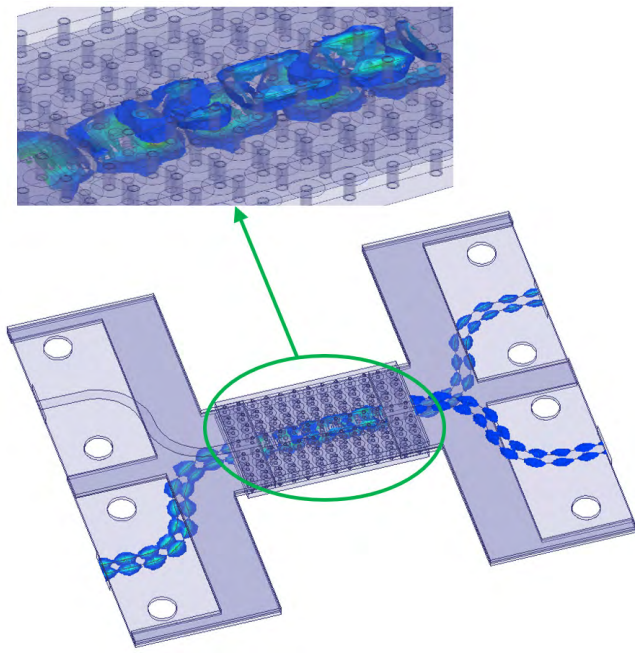

FIGURE 12. Magnitude of the travelling electric fields.

Fig. 12 shows the travelling waves inside the coupler. The simulated scattering parameters of the proposed ridge-gap coupler are carried out using HFSS (Fig. 13). As it can be seen from Fig. 13, the insertion loss in the operating bandwidth (57GHz to 64GHz) is lower than 3.5dB, which shows the very low-loss nature of the proposed ridge-gap coupler.

V. EXPERIMENTAL RESULTS

Fig. 14 shows a photo of the fabricated coupler. For measuring the fabricated coupler, we need to consider the connector response and length of the feeding microstrip transmission lines in the calibration procedure. Fig. 15 shows the frequency response of the connectors and feeding microstrip lines.

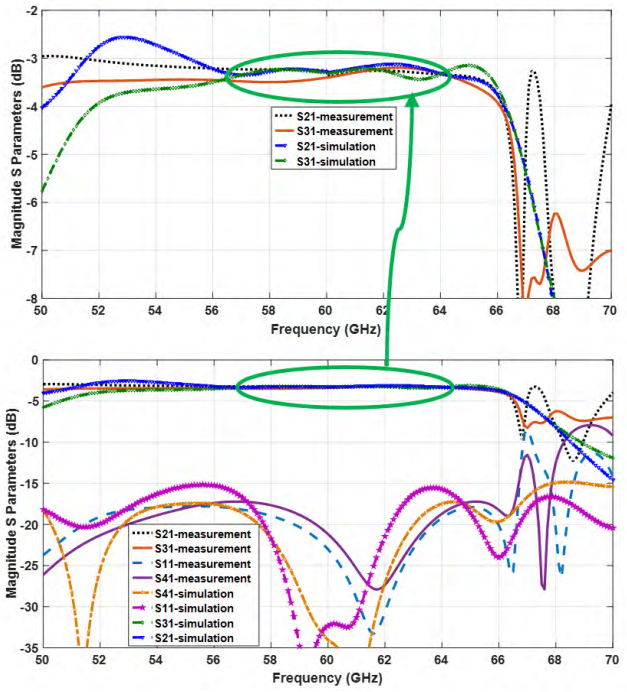

FIGURE 13. Measured and simulated results of the proposed ride-gap 3dB 90° hybrid coupler.

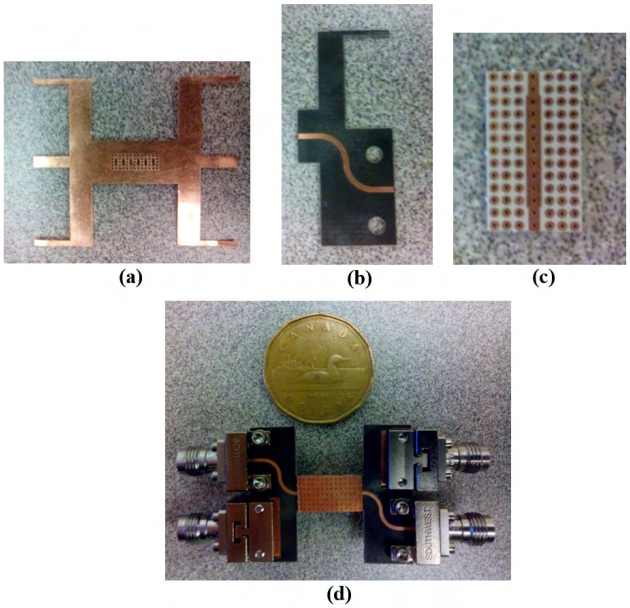

FIGURE 14. Photo of the fabricated proposed ridge-gap coupler. (a) Coupling wall. (b) Feeding microstrip line. (c) Host ridge-gap. (d) Proposed ridge-gap coupler.

A connector (1.85mm end lunch connector with part number of 1892-03A-5 from Southwest-Microwave Inc.) is used to test the proposed coupler. This connector works up to the frequency of 67GHz. The connector behavior is not given above this frequency by the company. Thus the circuit in Fig. 15(a) is used to see the connector response at higher frequency and also calibrating the measurement equipment. As it can be seen from Fig. 15(b), in the frequencies lower

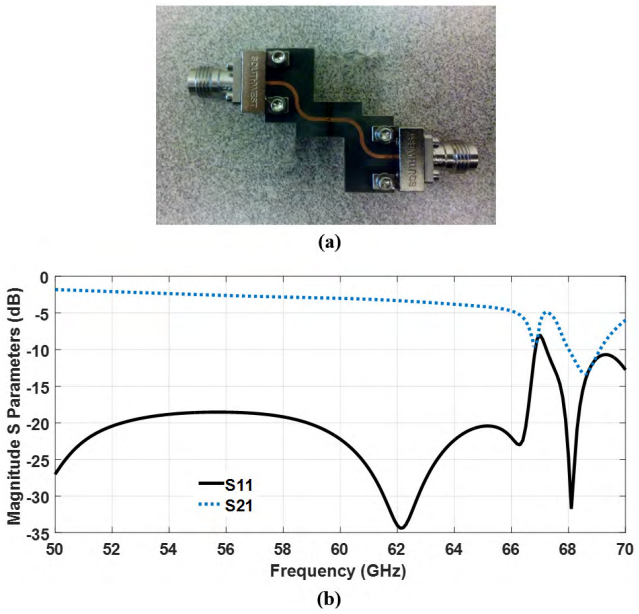

FIGURE 15. Test setup for measuring the connector and feeding microstrip line responses. (a) Test circuit. (b) Measurement results.

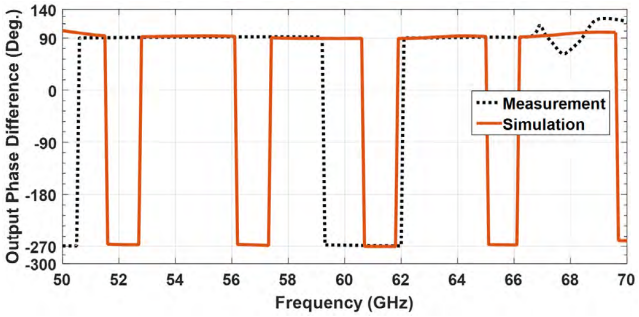

FIGURE 16. Output phase response of the proposed ride-gap 90° hybrid coupler.

than 66GHz, we have 2dB to 5dB loss, which is due to the feeding microstrip line at these frequencies. In the frequencies around 67GHz, there are some resonances which are due to the connector response. This behavior can be seen in the measurement results in Fig. 13. In this figure, the losses due to the microstrip feeding lines and connectors are taken into account by calibrating the measurement equipment. The output phase response of the proposed coupler is shown in Fig. 16. Some of the coupler parameters are compared with the equivalent presented couplers in the literature in Table 1. As it can be seen from this table, the first unique advantage of this technology is the low-loss nature of the ridge-gap transmission line. For instance, the insertion loss is lower than 3. 5dB in the operating frequency-band (57GHz to 64GHz). The second advantage of this design is the output phase error, which is lower than 1 degree in the operating frequency-band.

VI. CONCLUSION

A novel millimeter-wave 3dB 90° hybrid coupler fabricated with ridge-gap technology has been designed in this paper.

TABLE 1. Proposed Ridge-Gap Coupler Compared With Other Equivalent Presented Coupler in Literatures.

	Operating Frequency Band	Maximum Insertion loss	Maximum output phase error (degree)
Proposed ridge-gap coupler	57-64 GHz	3.5dB	1
Ref [3]	93-95 GHz	5.2dB	3
Ref [5]	9-11 GHz	3.9dB	2.6
Ref [6]	11-14 GHz	3.95dB	2.15

The dispersion diagram of the proposed ridge-gap transmission line has been extracted, and a transition to the microstrip transmission line has been presented. The multi-coupling aperture technique has been used for designing the coupler. The formulas have been developed to model the large coupling apertures where Bethe's small-aperture coupling theory does not lead to a good prediction. The phase response of the large coupling apertures have been used to compensate for the output progressive phase of the coupler. The proposed coupler has a very low insertion loss at millimeter-wave frequency range. It has been explained that why the proposed ridge-gap coupler has a very low insertion loss compared to the other millimeter-wave couplers made with other technologies such as SIW or microstrip.

APPENDIX

A. CALCULATE THE COUPLING

P_3 can be extracted by substituting A_n and C_n in (2), with assuming that C_n are equal to b_n which are equal for the six apertures ($C_n = b_n = C$).

$$P_3 = A_1 C e^{-j\beta 5S} + A_2 C e^{-j\beta 4S} + A_3 C e^{-j\beta 3S} + A_4 C e^{-j\beta 2S} + A_5 C e^{-j\beta S} + A_1 C \quad (14)$$

By substituting A_n from (4) into (14), we have

$$P_3 = P_1 C e^{-j\beta 5S}[1 + (1-2C) + (1-2C)^2 + (1-2C)^3 + (1-2C)^4 + (1-2C)^5] \quad (15)$$

The finite geometric series has the following simple formula

$$1 + x + x^2 + x^3 + x^4 + \ldots + x^n = \frac{1 - x^{n+1}}{1 - x} \quad (16)$$

$$\xrightarrow{\textit{Simplifying (15) using (16)}} P_3 = P_1 e^{-j\beta 5S}\left[\frac{1-(1-2C)^6}{2}\right] \quad (17)$$

By substituting C from (5) into (17), we have (18), as shown at the top of the next page.

B. CALCULATE THE OUTPUT PHASE DIFFERENCE

The phase difference between the two output ports (θ) is given by (9). P_2 can be written as

$$\xrightarrow{\textit{from (1) and (4)}} P_2 = P_1 (1-2C)^6 e^{-j\beta 6S} \quad (19)$$

$$Coupling = 10\log\left|\frac{P3}{P1}\right| = 10\log\left|\frac{1-\left(1-1.016\times W_s^3\times\frac{\tan\left(\frac{\pi f}{2f_{co}}\right)}{\frac{\pi f}{2f_{co}}}e^{\left(-\frac{2\pi h_m f_{co}Q}{C_0}\sqrt{1-\left(\frac{f}{f_{co}}\right)^2}\right)}\right)^6}{2}\right| \tag{18}$$

$$\theta = \beta S + \angle\left[\frac{1-\left(1-2\times 0.508\times W_s^3\times\frac{\tan\left(\frac{\pi f}{2f_{co}}\right)}{\frac{\pi f}{2f_{co}}}e^{\left(-\frac{2\pi h_m f_{co}Q}{C_0}\sqrt{1-\left(\frac{f}{f_{co}}\right)^2}\right)}\right)^6}{2\left(1-2\times 0.508\times W_s^3\times\frac{\tan\left(\frac{\pi f}{2f_{co}}\right)}{\frac{\pi f}{2f_{co}}}e^{\left(-\frac{2\pi h_m f_{co}Q}{C_0}\sqrt{1-\left(\frac{f}{f_{co}}\right)^2}\right)}\right)^6}\right] \tag{21}$$

$$\xrightarrow{\substack{\text{substituting } P_3 \text{ and } P_2 \text{ in (9)}\\ \text{by (17) and (19)}}} \theta = \beta S + \angle\left[\frac{1-(1-2C)^6}{2(1-2C)^6}\right] \tag{20}$$

By substituting C from (5) in (20), (21) can be achieved for the output phase difference, as shown at the top of this page.

REFERENCES

[1] X. Zou, F. Z. Geng, Y. Li, and Y. Leng, "Phase inverters based on substrate integrated waveguide," *IEEE Microw. Wireless Compon. Lett.*, vol. 27, no. 3, pp. 227–229, Mar. 2017.

[2] S. Wang, D. Zhang, Y. Zhang, L. Qing, and D. Zhou, "Novel dual-mode bandpass filters based on SIW resonators under different boundaries," *IEEE Microw. Wireless Compon. Lett.*, vol. 27, no. 1, pp. 28–30, Jan. 2017.

[3] E. Moldovan, R. G. Bosisio, and K. Wu, "W-band multiport substrate-integrated waveguide circuits," *IEEE Trans. Microw. Theory Techn.*, vol. 54, no. 2, pp. 625–632, Feb. 2006.

[4] G. Li, K. Song, F. Zhang, and Y. Zhu, "Novel four-way multilayer SIW power divider with slot coupling structure," *IEEE Microw. Wireless Compon. Lett.*, vol. 25, no. 12, pp. 799–801, Dec. 2015.

[5] T. Djerafi, K. Wu, and S. O. Tatu, "3 dB 90° hybrid quasi-optical coupler with air field slab in SIW technology," *IEEE Microw. Wireless Compon. Lett.*, vol. 24, no. 4, pp. 221–223, Apr. 2014.

[6] A. A. M. Ali, H. B. El-Shaarawy, and H. Aubert, "Compact wideband double-layer half-mode substrate integrated waveguide 90° deg coupler," *Electron. Lett.*, vol. 47, no. 10, pp. 598–599, May 2011.

[7] A. Polemi, S. Maci, and P.-S. Kildal, "Dispersion characteristics of a metamaterial-based parallel-plate ridge gap waveguide realized by bed of nails," *IEEE Trans. Antennas Propag.*, vol. 59, no. 3, pp. 904–913, Mar. 2011.

[8] H. Raza, J. Yang, P. S. Kildal, and E. A. Alós, "Microstrip-ridge gap waveguideŰstudy of losses, bends, and transition to WR-15," *IEEE Trans. Microw. Theory Techn.*, vol. 62, no. 9, pp. 1943–1952, Sep. 2014.

[9] A. U. Zaman, T. Vukusic, M. Alexanderson, and P. S. Kildal, "Design of a simple transition from microstrip to ridge gap waveguide suited for MMIC and antenna integration," *IEEE Antennas Wireless Propag. Lett.*, vol. 12, pp. 1558–1561, 2013.

[10] B. Liu, W. Hong, Y. Zhang, J. X. Chen, and K. Wu, "Half-mode substrate integrated waveguide (HMSIW) double-slot coupler," *Electron. Lett.*, vol. 43, no. 2, pp. 113–114, Jan. 2007.

[11] A. Ali, H. Aubert, N. Fonseca, and F. Coccetti, "Wideband two-layer SIW coupler: Design and experiment," *Electron. Lett.*, vol. 45, no. 13, pp. 687–689, Jun. 2009.

[12] R. Levy, "Improved single and multiaperature waveguide coupling theory, including explanation of mutual interactions," *IEEE Trans. Microw. Theory Techn.*, vol. 28, no. 4, pp. 331–338, Apr. 1980.

[13] H. Schmiedel, "Series-configuration of multi-line directional-coupler sections with improved coupling," in *IEEE MTT-S Int. Microw. Symp. Dig.*, Jun. 2004, pp. 339–342.

[14] S. B. Cohn, "Microwave coupling by large apertures," *Proc. IRE*, vol. 40, no. 6, pp. 696–699, Jun. 1952.

MOHAMMADMAHDI FARAHANI received the Diploma degree in electrical engineering, applied electromagnetisms engineering from Iran University of Science and Technology (IUST), Tehran, Iran, in 2012. He is currently pursuing the Ph.D. degree with the Institut National de la Recherche Scientifique, Université du Québec, Montreal, QC, Canada. From 2009 to 2012, he was a Researcher with the IUST Antennas and Microwave Research Laboratory, RF Communications' Systems Group. His current research interests include phase array antennas, adaptive arrays, switched multibeam antenna arrays, FSS structures, dielectric resonator antennas, metamaterial antennas, and microwave components development for wireless communications systems.

MOHAMMAD AKBARI received the B.Sc. degree in engineering-telecommunication from the University of Shahid Bahonar, Kerman, Iran, in 2007, and the M.Sc. degree in electrical engineering-telecommunication from the University of Urmia, Urmia, Iran, in 2011. He is currently pursuing the Ph.D. degree with Concordia University, Montreal, Canada. He has taught courses in microwave engineering, antenna theory, and fields and waves, and electromagnetics in Aeronautical University, Tehran, Iran. His main field of research includes analysis and design of microstrip antennas, modeling of microwave structures, electromagnetic theory and analysis of UWB antennas for WBAN applications, antenna interactions with the human body, mm-wave technology, phased and switched-beam arrays, microstrip antennas and circuits, sequential feedings, periodic structures and their application to antenna design, and performance enhancement. He has authored or co-authored approximately 50 peer-reviewed scientific journals and international conference articles. He received the Graduate Concordia Merit Scholarship.

MOURAD NEDIL (M'08–SM'12) received the Dipl.-Ing. degree from the University of Algiers, Algiers, Algeria, in 1996, the D.E.A (M.S.) degree from the University of Marne la Vallée, Marne la Vallée, France, in 2000, and the Ph.D. degree from the Institut National de la Recherche Scientifique (INRS-EMT), Université de Québec, Montreal, QC, Canada, in 2006. From 2006 to 2008, he completed a Postdoctoral Fellowship with the RF Communications Systems Group, INRS-EMT. In 2008, he joined the Engineering School Department, Université de Québec en Abitibi-Témiscamingue, Rouyn-Noranda, QC, Canada, where he is currently an Associate Professor. His current research interests include antennas, multiple-input and multiple-output radio-wave propagation, and microwave devices.

TAYEB A. DENIDNI (M'98–SM'04) received the M.Sc. and Ph.D. degrees in electrical engineering from Laval University, Quebec City, QC, Canada, in 1990 and 1994, respectively.

From 1994 to 2000, he was a Professor with the Engineering Department, Université du Québec at Rimouski, Rimouski, QC, Canada, where he founded the Telecommunications Laboratory. Since 2000, he has been with the Institut National de la Recherche Scientifique (INRS), Université du Québec, Montreal, QC, Canada. He found the RF Laboratory, INRS-EMT, Montreal. He has extensive experience with antenna design and is leading a large research group consisting of three research scientists, six Ph.D students, and one M.Sc. student. He served as a Principal Investigator on many research projects sponsored by NSERC, FCI, and numerous industries. His current research areas of interest include reconfigurable antennas using EBG and FSS structures, dielectric resonator antennas, metamaterial antennas, adaptive arrays, switched multibeam antenna arrays, ultra-wideband antennas, microwave and development for wireless communications systems.

From 2008 to 2010, Dr. Denidni served as an Associate Editor of the IEEE TRANSACTIONS ON ANTENNAS PROPAGATION. From 2005 to 2007, he served as an Associate Editor of the IEEE ANTENNAS WIRELESS PROPAGATION LETTERS. Since 2015, he has been serving as an Associate Editor of the *IET Electronics Letters*. In 2012 and 2013, he received the Outstanding Research and Teaching Achievements Awards from INRS.

ABDEL R. SEBAK (F'10) received the B.Sc. degree (Hons.) in electrical engineering from Cairo University, Cairo, Egypt, in 1976, the B.Sc. degree in applied mathematics from Ein Shams University, Cairo, in 1978, and the M.Eng. and Ph.D. degrees in electrical engineering from the University of Manitoba, Winnipeg, MB, Canada, in 1982 and 1984, respectively.

From 1984 to 1986, he was with Canadian Marconi Company, where he was involved in the design of microstrip phased array antennas. From 1987 to 2002, he was a Professor with the Department of Electronics and Communication Engineering, University of Manitoba. He is currently a Professor with the Department of Electrical and Computer Engineering, Concordia University, Montreal, QC, Canada. His research interests include phased array antennas, millimeter-wave antennas and imaging, computational electromagnetics, and interaction of EM waves with engineered materials and bioelectromagnetics.

Prof. Sebak has served as the Chair of the IEEE Canada Awards and Recognition Committee from 2002 to 2004 and as the Technical Program Chair of the 2002 IEEE CCECE Conference and the 2006 URSIANTEM Symposium. He is the Technical Program Cochair of the 2015 IEEE ICUWB Conference. He is a member of the Canadian National Committee of International Union of Radio Science Commission B. He received the 1992 and 2000 University of Manitoba Merit Award for Outstanding Teaching and Research, the 1994 Rh Award for Outstanding Contributions to Scholarship and Research, and the 1996 Faculty of Engineering Superior.